# Bottomonium decay matrix elements from lattice QCD with two light quarks

G. T. Bodwin and D. K. Sinclair
*HEP Division, Argonne National Laboratory, 9700 South Cass Avenue, Argonne, Illinois 60439*

S. Kim
*Physics Department, Sejong University, Seoul 143-747, Korea*
(Received 13 July 2001; published 31 January 2002)

We calculate the long-distance matrix elements for the decays of the $\Upsilon(\eta_b)$ and $\chi_b$ $(h_b)$ states in lattice QCD with two flavors of light dynamical quarks. We relate the lattice matrix elements to their continuum counterparts through one-loop order in perturbation theory. In the case of the leading *S*-wave matrix element, we compare our result with a phenomenological value that we extract from the experimental leptonic decay rate by using the theoretical expression for the decay rate, accurate through relative order $\alpha_s$. Whereas estimates of the leading *S*-wave matrix element from quenched QCD are 40–45 % lower than the phenomenological value, the two-flavor estimate of the same matrix element is close to the phenomenological value. Extrapolating to the real world of $2+1$ light flavors, we find that this matrix element is approximately 6% higher than the phenomenological value, but that the phenomenological value lies within our error bars. We also compute the color-singlet and color-octet matrix elements for *P*-wave decays. We find the value of the color-singlet matrix element for $2+1$ flavors to be approximately 70% larger than the quenched value and the value of the color-octet matrix element for $2+1$ flavors to be approximately 40% larger than the quenched value.

DOI: 10.1103/PhysRevD.65.054504 PACS number(s): 12.38.Gc, 13.25.Gv

## I. INTRODUCTION

Bottomonium is a nonrelativistic system: the velocity $v$ of the $b$ and $\overline{b}$ quarks in the center-of-mass frame is much less than unity ($v^2 \approx 0.1$). Bodwin, Braaten and Lepage [1] have shown that, within the framework of nonrelativistic quantum chromodynamics (NRQCD), the smallness of $v$ allows one to expand the decay rates into light hadrons and/or electromagnetic decay products in powers of $v$. Each term in this velocity expansion can be expressed as a finite number of terms, each of which is a product of a long-distance ($\sim 1/M_b v$) matrix element of a four-fermion operator between bottomonium states and a short-distance ($\sim 1/M_b$) parton-level decay rate. Owing to the asymptotic freedom of QCD, the short-distance parton-level decay rate can be calculated perturbatively.

The *S*-wave bottomonium decay rates can be expressed, through next-to-leading order in $v^2$, as

$$\Gamma(^{2s+1}S_{2s+1} \to X) = \mathcal{G}_1(^{2s+1}S_{2s+1})\, 2\,\mathrm{Im}\, f_1(^{2s+1}S_{2s+1})/M_b^2 + \mathcal{F}_1(^{2s+1}S_{2s+1})\, 2\,\mathrm{Im}\, g_1(^{2s+1}S_{2s+1})/M_b^4 . \quad (1)$$

Similarly the *P*-wave bottomonium decay rates at lowest non-trivial order in $v$ are given by

$$\Gamma(^{2s+1}P_J \to X) = \mathcal{H}_1(^{2s+1}P_J)\, 2\,\mathrm{Im}\, f_1(^{2s+1}P_J)/M_b^4 + \mathcal{H}_8(^{2s+1}P_J)\, 2\,\mathrm{Im}\, f_8(^{2s+1}S_{2s+1})/M_b^2 . \quad (2)$$

The $f$'s and $g$'s are proportional to the short-distance rates for the annihilation of a $b\overline{b}$ pair from the indicated $^{2s+1}L_J$ state, while $\mathcal{G}_1$, $\mathcal{F}_1$, $\mathcal{H}_1$, and $\mathcal{H}_8$ are the long-distance matrix elements.[1] The subscripts 1 and 8 indicate that the $b\overline{b}$ pair is in a relative color-singlet or color-octet state. If one works to leading order in $v$ in the NRQCD Lagrangian, then the matrix elements of the spin-singlet and spin-triplet states are equal.

In earlier papers [3], we reported lattice NRQCD calculations of $\mathcal{G}_1$, $\mathcal{F}_1$, $\mathcal{H}_1$, and $\mathcal{H}_8$ for the $\Upsilon(\eta_b)$ and $\chi_b$ $(h_b)$ states that made use of quenched gauge-field configurations with inverse lattice spacings $a^{-1} \approx 2.4$ GeV and $a^{-1} \approx 1.37$ GeV. We found that the value of the best-measured matrix element $\mathcal{G}_1$ is 40–45 % below a phenomenological value that we extracted from the leptonic width of the $\Upsilon$ and the theoretical expression for the width, accurate through relative order $\alpha_s$.[2] The NRQCD Collaboration [4,5] had noted that at least part of the discrepancy is likely due to the use of the quenched approximation. The reason that the quenched approximation underestimates the matrix element is that the distance scale associated with the bottomonium bound state [order $1/(M_b v)$] is considerably larger than the scale at which the matrix elements sample the wave function (order $a$, which is order $1/M_b$). If we fix the lattice QCD coupling at $1/(M_b v)$ to a value that yields good agreement with the bottomonium spectrum, then, in the quenched approximation, the coupling at $a$ will be weaker than it should be. Hence, the wave function at the origin will be too small, leading to a prediction for the bottomonium decay rate that is too small.

[1] Our quantities $\mathcal{H}_1$ and $\mathcal{H}_8$ are related to the quantities $H_1$ and $H_8$ in Ref. [2] by $\mathcal{H}_1 = M_b^4 H_1$ and $\mathcal{H}_8 = M_b^2 H_8$.

[2] The phenomenological value that we quote in the present paper is based on a slightly different value for $\alpha_s$ than was used in Ref. [3].

 

In this paper we present calculations of the decay matrix elements for the $\Upsilon(\eta_b)$ and $\chi_b$ $(h_b)$ states that make use of gauge configurations containing the effects of two flavors of light dynamical (staggered) quarks. These calculations confirm that most, if not all, of the discrepancy in the previous calculations of the matrix elements was, in fact, due to quenching. Our results, when extrapolated to three light flavors, lead to a slight overestimate of the $\Upsilon$ decay rate.

The remainder of this paper is organized as follows. In Sec. II we define the required matrix elements in the continuum and on the lattice and describe the lattice implementation of NRQCD that we use in our calculations. Section III contains an outline of the perturbative calculation that we use to relate the lattice matrix elements to their continuum counterparts. We present our results in Sec. IV, and Sec. V contains our conclusions.

## II. MATRIX ELEMENTS AND LATTICE NRQCD

In the leading non-trivial order in $v$, the NRQCD Lagrangian for the bottom quark and antiquark is

$$\mathcal{L}_B = \psi^\dagger \left( D_t - \frac{\mathbf{D}^2}{2M_b} \right) \psi + \chi^\dagger \left( D_t + \frac{\mathbf{D}^2}{2M_b} \right) \chi, \tag{3}$$

where $\psi$ is the quark annihilation operator and $\chi$ is the antiquark creation operator. $D_t$ and $\mathbf{D}$ are the gauge-covariant temporal and spatial derivatives. Note that, although one can obtain the correct leading-order spectroscopy in the Coulomb gauge by replacing $\mathbf{D}$ with the simple (non-covariant) gradient operator, the covariant operator is needed to calculate the octet $P$-wave decay matrix element, even at lowest non-trivial order. Not surprisingly, Eq. (3) is just the Euclidean-time Schrödinger Lagrangian for the bottom quarks and antiquarks.

We work to leading order in $v$ in the Lagrangian. As we have mentioned, at this order, the matrix elements of the spin-triplet and spin-singlet states are identical. Therefore, we approximate all of the long-distance matrix elements in Eqs. (1) and (2) as spin-singlet matrix elements. Using the leading-order Lagrangian, we are able to compute the order-$v^2$ $S$-wave matrix element $\mathcal{F}_1$, with an error of order $v^4$. Note, however, that, in order to obtain a full relative-order-$v^2$ computation of the $S$-wave decay rate, we would need to compute $\mathcal{G}_1$ through relative-order $v^2$. This would require relative-order-$v^2$ terms in the Lagrangian, in which case the spin-singlet and spin-triplet states would be distinguished.

In terms of the fields $\chi$ and $\psi$, the spin-singlet matrix elements that we compute are

$$\mathcal{G}_1 = \langle\, ^1S_0 | \psi^\dagger \chi \chi^\dagger \psi |\, ^1S_0 \rangle, \tag{4a}$$

$$\mathcal{F}_1 = \langle\, ^1S_0 | \psi^\dagger \chi \chi^\dagger \left( -\frac{i}{2} \overleftrightarrow{\mathbf{D}} \right)^2 \psi |\, ^1S_0 \rangle, \tag{4b}$$

$$\mathcal{H}_1 = \langle\, ^1P_1 | \psi^\dagger (i/2) \overleftrightarrow{\mathbf{D}} \chi \cdot \chi^\dagger (i/2) \overleftrightarrow{\mathbf{D}} \psi |\, ^1P_1 \rangle, \tag{4c}$$

$$\mathcal{H}_8 = \langle\, ^1P_1 | \psi^\dagger T^a \chi \chi^\dagger T^a \psi |\, ^1P_1 \rangle, \tag{4d}$$

where $\chi^\dagger \overleftrightarrow{\mathbf{D}} \psi \equiv \chi^\dagger \mathbf{D} \psi - (\mathbf{D}\chi)^\dagger \psi$.

The vacuum-saturation approximation is valid for the color-singlet matrix elements and is accurate up to errors of relative order $v^4$ (Ref. [1]). In that approximation, Eqs. (4a), (4b), and (4c) become

$$\mathcal{G}_1 \approx \mathcal{G}_1^{\rm VS} = \langle\, ^1S_0 | \psi^\dagger \chi | 0 \rangle \langle 0 | \chi^\dagger \psi |\, ^1S_0 \rangle, \tag{5a}$$

$$\mathcal{F}_1 \approx \mathcal{F}_1^{\rm VS} = \langle\, ^1S_0 | \psi^\dagger \chi | 0 \rangle \langle 0 | \chi^\dagger \left( -\frac{i}{2} \overleftrightarrow{\mathbf{D}} \right)^2 \psi |\, ^1S_0 \rangle, \tag{5b}$$

$$\mathcal{H}_1 \approx \mathcal{H}_1^{\rm VS} = \langle\, ^1P_1 | \psi^\dagger (i/2) \overleftrightarrow{\mathbf{D}} \chi | 0 \rangle \cdot \langle 0 | \chi^\dagger (i/2) \overleftrightarrow{\mathbf{D}} \psi |\, ^1P_1 \rangle. \tag{5c}$$

One can express vacuum-saturation values of the color-singlet matrix elements as $\mathcal{G}_1^{\rm VS} = (3/2\pi)|R_S(0)|^2$ and $\mathcal{H}_1^{\rm VS} = (9/2\pi)|R_P'(0)|^2$, where $R_S(0)$ is the radial wave function of the $S$-wave state at the origin and $R_P'(0)$ is the derivative of the radial $P$-wave wave function at the origin [1]. These are the quantities that appear in decay rates in the color-singlet model. In contrast, the term proportional to $\mathcal{H}_8$ is absent in decay rates in the color-singlet model. $\mathcal{H}_8$ is the probability of finding a $b\bar{b}g$ component in $P$-wave bottomonium, with the $b\bar{b}$ in a color-octet state.

In our lattice calculation of these matrix elements, we transform our gauge field configurations to the Coulomb gauge. For this gauge choice, we can replace the covariant $\mathbf{D}$ with the non-covariant $\boldsymbol{\nabla}$ in Eq. (4). Corrections to this replacement are suppressed by $v^2$.

We employ various discretizations of the derivative operator. For the operator $\mathcal{H}_1$, we replace the covariant derivative $\mathbf{D}$ with the non-covariant finite difference $\boldsymbol{\delta}$, which is defined by

$$\delta_i \psi(x) = \frac{1}{2} [\, \psi(x + \mathbf{i}) - \psi(x - \mathbf{i}) \,], \tag{6}$$

where $\mathbf{i}$ is the unit vector in the $i$th spatial direction. For $\mathcal{F}_1$ we employ four different discretizations of $\mathbf{D}^2$:

$$\Delta^{(2)}(\text{non})\, \psi(x) = \sum_i \, [\, \psi(x + \mathbf{i}) + \psi(x - \mathbf{i}) - 2\psi(x) \,], \tag{7a}$$

$$\Delta^{(2)}(\text{cov})\, \psi(x) = \sum_i \, \left\{ \frac{1}{u_0} [\, U_i(x)\, \psi(x + \mathbf{i}) + U_i^\dagger(x - \mathbf{i})\, \psi(x - \mathbf{i}) \,] - 2\psi(x) \right\}, \tag{7b}$$

$$\psi^\dagger \Delta^{(2)}(\text{non}_2) \chi = -\sum_i \, [\, (\delta_i \psi)^\dagger \delta_i \chi \,], \tag{7c}$$

$$\psi^\dagger \Delta^{(2)}(\text{cov}_2) \chi = -\sum_i \, [\, (d_i \psi)^\dagger d_i \chi \,], \tag{7d}$$

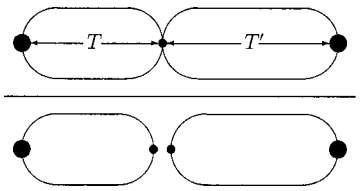


FIG. 1. Lattice calculation of a matrix element of a four-fermion operator. The large discs represent the sources and sinks; the smaller discs represent the four-fermion and point source operators. The lines are the nonrelativistic quark propagators.

where the covariant finite difference $d$ is defined by

$$d_i\psi(x)=\frac{1}{2u_0}[U_i(x)\psi(x+\mathbf{i})-U_i^\dagger(x-\mathbf{i})\psi(x-\mathbf{i})], \quad (8)$$

and $u_0$ is the tadpole contribution to $U$. We adopt the definition $u_0=\langle\frac{1}{3}U_{\rm plaq}\rangle^{1/4}$.

On the lattice, we obtain such matrix elements by measuring the expectation value in the gluon background of a product of three operators: a source for a $b\bar{b}$ pair with the appropriate quantum numbers at a (Euclidean) time $-T$, the appropriate four-fermion operator at time zero, and a sink for the $b\bar{b}$ pair at time $T'$. For convenience, and in order to reduce noise, we divide this expectation value by the product of two other expectation values. One is the expectation value of the product of the numerator source for the $b\bar{b}$ pair at time $-T$ and a point sink that annihilates the $b\bar{b}$ pair at time zero; the other is the expectation value of the product of a point source that creates a $b\bar{b}$ pair at time zero and the numerator sink, which annihilates the $b\bar{b}$ pair at time $T'$. This ratio is illustrated in Fig. 1.

In the cases of $\mathcal{G}_1$ and $\mathcal{H}_1$, this ratio approaches the ratio of the matrix element to its vacuum-saturation approximation in the limit $T,T'\to\infty$. Hence, it gives an indication of the accuracy of the vacuum-saturation approximation. In the case of $\mathcal{H}_8$, this ratio yields $\mathcal{H}_8/\mathcal{H}_1^{\rm VS}$ in the limit $T,T'\to\infty$. We obtain values for $\mathcal{G}_1$ and $\mathcal{H}_1$ in the vacuum-saturation approximation from the relations

$$\sum_x \langle 0|\chi^\dagger(x,T)\psi(x,T)\psi^\dagger(0,0)\chi(0,0)|0\rangle \overset{T\to\infty}{\to} \mathcal{G}_1^{\rm VS}\exp(-E_S T) \quad (9)$$

and

$$\sum_x \langle 0|\chi^\dagger(x,T)\left(-\frac{i}{2}\overleftrightarrow{\mathbf{D}}\right)\psi(x,T)\cdot\psi^\dagger(0,0)\left(-\frac{i}{2}\overleftrightarrow{\mathbf{D}}\right)\chi(0,0)|0\rangle \overset{T\to\infty}{\to} \mathcal{H}_1^{\rm VS}\exp(-E_P T), \quad (10)$$

which follow from the fact that only the lowest-lying intermediate state with the correct quantum numbers contributes to the amplitude in the limit $T\to\infty$. Note that we can write

$$\mathcal{G}_1^{\rm VS}=a_p^2, \quad (11)$$

where one factor of $a_p$ is from the point source and the other is from the point sink. If we replace the point source by another (extended) source, the coefficient of the exponential is of the form $a_p a_x$, while if we use this new extended-source operator for both source and sink, the coefficient is $a_x^2$. Thus, introducing an extended source which has a greater overlap with the ground state gives us an alternative method of extracting $a_p$ and, hence, $\mathcal{G}_1$. Similar comments hold for $\mathcal{H}_1$ and $\mathcal{F}_1$. We calculate the $\mathcal{F}_1$'s from

$$\frac{-\sum_x \langle 0|\chi(x,T)^\dagger\Delta^{(2)}(*)\psi(x,T)S(0)|0\rangle}{\sum_x \langle 0|\chi(x,T)^\dagger\psi(x,T)S(0)|0\rangle} \overset{T\to\infty}{\to} \frac{\mathcal{F}_1^{\rm VS}}{\mathcal{G}_1^{\rm VS}}, \quad (12)$$

where $\Delta^{(2)}(*)$ denotes any of the discretizations of $\mathbf{D}^2$ in Eq. (7), and $S(0)$ is any source with a finite overlap with the lowest $S$-wave state on time slice 0.

In order to evaluate these matrix elements, we must calculate bottom-quark propagators $G(x;y)$ on the lattice. Following Lepage *et al.* [6], we calculate the retarded propagator $G_r(\mathbf{x},t;0)$ by iterating the equation

$$G_r(\mathbf{x},x_0+1;0)=(1-H_0/2n)^n U^\dagger_{\mathbf{x},x_0}(1-H_0/2n)^n G_r(\mathbf{x},x_0;0) + \delta_{\mathbf{x},\mathbf{0}}\delta_{x_0+1,0}, \quad (13)$$

setting $G(\mathbf{x},x_0;0)=0$ for $x_0<0$. In Eq. (13), $H_0=-\Delta^{(2)}/2M_0-h_0$, $\Delta^{(2)}$ is the gauge-covariant discrete Laplacian, which is given by the expression in Eq. (7b) with $u_0$ set to unity, $h_0=3(1-u_0)/M_0$, and $M_0$ is the bare bottom-quark mass. We note that our bare bottom-quark mass is defined to be $u_0$ times that of Ref. [7]. The value two for the discretization parameter $n$ turns out to be adequate for our calculations.

An expression that is similar to Eq. (13) exists for the advanced propagator $G_a$. The relation $G_r(x;y)=G_a^\dagger(y;x)$ makes it possible to rewrite amplitudes, interchanging sources and sinks. Such a rewriting allows one to start all propagator calculations from a noisy (point or extended) source, rather than a point source and, thereby, to reduce both the statistical error and the number of calculational steps.

## III. THE RELATIONSHIP BETWEEN LATTICE AND CONTINUUM MATRIX ELEMENTS

We wish to relate our lattice results to the continuum [modified minimal subtraction scheme ($\overline{\rm MS}$)] matrix elements that are used in phenomenology. Lattice matrix elements and continuum matrix elements differ only in the choice of ultraviolet regulator. Furthermore, a change of ul-

traviolet regulator is dependent only on the large-momentum (short-distance) parts of an amplitude. Consequently, asymptotic freedom allows us to compute the short-distance coefficients that relate the lattice matrix elements to the continuum matrix elements in a perturbation series in the strong coupling $\alpha_s$. The short-distance coefficients are independent of the hadronic state. Therefore, for purposes of computing the short-distance coefficients, we choose, for convenience, to evaluate the operators in free $Q\overline{Q}$ states.

We can expand the lattice-regulated matrix element of an operator in terms of continuum-regulated matrix elements of a complete set of operators:

$$\langle \mathcal{O}_i \rangle_L = \sum_j c_{ij} \langle \mathcal{O}_j \rangle_C , \tag{14}$$

where the $c_{ij}$ are the short-distance coefficients, $\langle \mathcal{O} \rangle$ is the matrix element of the operator $\mathcal{O}$ in a free $Q\overline{Q}$ state, and the subscripts $L$ and $C$ indicate the lattice- and continuum-regulated matrix elements, respectively. The matrix elements and short-distance coefficients can be expanded in perturbation series:

$$\langle \mathcal{O}_i \rangle_L = \langle \mathcal{O}_i \rangle_L^{(0)} + \alpha_s \langle \mathcal{O}_i \rangle_L^{(1)} + \cdots , \tag{15a}$$

$$\langle \mathcal{O}_i \rangle_C = \langle \mathcal{O}_i \rangle_C^{(0)} + \alpha_s \langle \mathcal{O}_i \rangle_C^{(1)} + \cdots , \tag{15b}$$

$$c_{ij} = c_{ij}^{(0)} + \alpha_s c_{ij}^{(1)} + \cdots . \tag{15c}$$

For simplicity, we use the same definition of $\alpha_s$ and the same scale for $\alpha_s$ in all three expansions in Eq. (15).

At zeroth order in the perturbation series, the momentum-space expression for a lattice operator is equal to the momentum-space expression for the corresponding continuum operator, plus terms of higher order in the lattice spacing $a$ times the momenta. Therefore,

$$c_{ii}^{(0)} = 1, \tag{16}$$

and

$$c_{ij}^{(0)} = 0 \quad \text{for } \mathrm{Dim}\,\mathcal{O}_j < \mathrm{Dim}\,\mathcal{O}_i , \tag{17}$$

where $\mathrm{Dim}\,\mathcal{O}$ is the mass dimension (or, equivalently, order in $v$) of the operator $\mathcal{O}$. For the operators that we consider in this paper,

$$c_{ij}^{(0)} = 0 \quad \text{for } i \neq j. \tag{18}$$

Since our lattice NRQCD action is accurate only to leading order in $v$, only the following mixings can be treated consistently: $\mathcal{G}_{1L}$ into $\mathcal{G}_{1C}$ and $\mathcal{F}_{1C}$, $\mathcal{F}_{1L}$ into $\mathcal{F}_{1C}$, $\mathcal{H}_{1L}$ into $\mathcal{H}_{1C}$ and $\mathcal{H}_{8C}$, and $\mathcal{H}_{8L}$ into $\mathcal{H}_{8C}$ and $\mathcal{H}_{1C}$. Therefore, we need consider, at most, two operators in the expansion (14). Then, using Eqs. (15), (16), and (18), we equate the terms of order $\alpha_s^1$ in Eq. (14) to obtain

$$\langle \mathcal{O}_i \rangle_L^{(1)} - \langle \mathcal{O}_i \rangle_C^{(1)} = c_{ii}^{(1)} \langle \mathcal{O}_i \rangle_C^{(0)} + c_{ij}^{(1)} \langle \mathcal{O}_j \rangle_C^{(0)} \quad \text{for } i \neq j, \tag{19}$$

where no sum over $j$ is implied. The quantities on the left side of Eq. (19) are computed in perturbation theory. We determine the short-distance coefficients on the right side of Eq. (19) by expanding the quantity on the left side of Eq. (19) in powers of the external $Q\overline{Q}$ 3-momenta and by choosing free $Q\overline{Q}$ states with particular color (and, in general, spin) quantum numbers.

In the expansion of the quantity on the left side of Eq. (19) in powers of the external $Q\overline{Q}$ 3-momenta, the various terms are infrared finite, to the extent that the behavior of the integrand in the lattice matrix element matches the behavior of the integrand in the continuum matrix element at small loop momentum. The expansions for the various mixings that we have mentioned above yield, at most, a linear infrared divergence in the lattice and continuum matrix elements. Since our lattice action (and, implicitly, our continuum action) are accurate to leading order in $v^2$, those divergences cancel between the lattice and continuum matrix elements on the left side of Eq. (19).

In general, infrared divergences in differences between lattice and continuum matrix elements cancel, provided that one works consistently to a given order in $v$. This means that, in order to compute coefficient of the mixing of a lattice matrix element into a continuum matrix element of relative order $v^n$, one must employ lattice and continuum actions that are accurate to relative order $v^n$. Then, the small-loop-momentum behaviors of the lattice and continuum contributions on the left side of Eq. (19) will be the same, and infrared divergences in the mixing coefficient will cancel. On the other hand, one should not compute operator mixings that exceed the accuracy in $v$ of the action. For example, since we use actions of leading order in $v$, we do not compute the one-loop correction to the mixing of $\mathcal{G}_{1L}$ into $\mathcal{F}_{1C}$ (relative order $v^2$). If one were to carry out such a computation, using the leading-order NRQCD lattice and continuum actions, then the expression for the one-loop correction would contain a cubic leading infrared divergence in both the lattice and continuum contributions on the left side of Eq. (19). The cubic leading divergence would cancel, but, owing to the absence of order-$v^2$ terms in the action, a linear subleading divergence would persist.

Applying Eqs. (14), (16), and (18) to the operator matrix elements that we consider in this paper, we obtain

$$\mathcal{G}_{1L} = (1+\epsilon)\mathcal{G}_1 , \tag{20a}$$

$$\mathcal{F}_{1L} = (1+\gamma)\mathcal{F}_1 + \phi\mathcal{G}_1 , \tag{20b}$$

and

$$\mathcal{H}_{1L} = (1+\iota)\mathcal{H}_1 + \kappa\mathcal{H}_8 , \tag{21a}$$

$$\mathcal{H}_{8L} = (1+\eta)\mathcal{H}_8 + \zeta\mathcal{H}_1 , \tag{21b}$$

where we have dropped the subscript $C$ on the continuum matrix elements, and the coefficients $\epsilon$, $\gamma$, $\phi$, $\iota$, $\kappa$, $\eta$ and $\zeta$ are of order $\alpha_s$. It turns out, in an explicit calculation,

that the coefficient $\kappa$ actually vanishes in order $\alpha_s$. Details of the calculations of these coefficients will be given elsewhere [8].

We note that the perturbation series for the $\overline{\rm MS}$ continuum short-distance coefficients that relate matrix elements to physical quantities contain renormalon ambiguities. The $\overline{\rm MS}$ continuum operator matrix elements contain compensating ambiguities, and, so, the physical quantities are ambiguity free [9]. In contrast, the lattice operator matrix elements and the short-distance coefficients that relate them to physical quantities are free of renormalon ambiguities [9]. Consequently, the perturbation series that relate the lattice and the $\overline{\rm MS}$ continuum operator matrix elements contain renormalon ambiguities. At the one-loop order to which we work, the factorial growth of the series associated with the presence of renormalons is unimportant. However, because the series that relate the lattice and the $\overline{\rm MS}$ continuum operator matrix elements (and the series that relate physical quantities and the $\overline{\rm MS}$ continuum operator matrix elements) ultimately fail to converge, the value of an $\overline{\rm MS}$ continuum matrix element is meaningful only if one specifies the order in perturbation theory that is employed in computing it.

## IV. RESULTS

### A. Lattice computation of the matrix elements

For the lattice calculations, we use gauge configurations generated by the HEMCGC Collaboration [10] with two flavors of light dynamical staggered quarks on a $16^3\times 32$ lattice at $\beta\equiv 6/g^2=5.6$. We use all 399 configurations with light-quark mass $m=0.01$ (in lattice units) and 200 configurations with quark mass $m=0.025$. As we have already mentioned, we follow Lepage *et al.* in choosing $u_0=[\frac{1}{3}{\rm Tr}\,U_{\rm plaq}]^{1/4}$ as our definition of the tadpole contribution to $U$. Our measurements yield $u_0=0.866985(11)$ at $m=0.01$ and $u_0=0.866773(12)$ at $m=0.025$. Since these are so close, we use 0.866859 for our perturbative calculations. We choose our bare bottom-quark mass to be $M_b=1.56\approx 1.80u_0$, where 1.80 is the value chosen by the NRQCD Collaboration [7] to yield the best fit to the $\Upsilon$-$\chi_b$ and $\Upsilon$-$\Upsilon'$ mass splittings.

To calculate the required matrix elements, we first gauge fix our configurations to the Coulomb gauge. We then generate the advanced and retarded bottom-quark propagators from a stochastic estimator to an $S$-wave point source, a stochastic estimator to an $S$-wave Gaussian source, and a stochastic estimator to a $P$-wave point source for each color on each time slice. The width of the Gaussian source is chosen to be 2.5 in lattice units, which is approximately the radius of $\Upsilon$ or $\eta_b$. From these we calculate the $S$- and $P$-wave bottomonium propagators, with both point and Gaussian sources and sinks, and the matrix elements of Fig. 1 and Eq. (12). Because the extended source has a larger overlap with the ground state than does the point source, we extract $a_x^2$ from fits of the propagator with an extended (Gaussian) source and sink to the form $a_x^2\exp(-ET)$ for large $T$. We then calculate the ratio $a_p/a_x$ from fits of the ratio of the propagator with extended source and point sink to the propagator with extended source and sink. Finally, we extract $\mathcal{G}_1(\mathcal{H}_1)=2a_0^2$. [An extra factor of two appears here relative to Eq. (11) because, owing to the spin independence of the lattice action at leading order in $v$, we compute propagators for only a single spin component.] In the case of $\mathcal{G}_1$, the direct extraction from the point-source–point-sink propagator gives a result that is consistent with this indirect method. However, for $\mathcal{H}_1$ the point-point propagator is very noisy and shows no sign of a plateau in the effective wave-function plot. In this case the indirect method is required. Figure 2 shows the effective wave function as a function of $T$ for the $S$-wave extended-extended propagator. Figure 3 shows the ratio of the $S$-wave extended-point propagator to the $S$-wave extended-extended propagator as a function of $T$.

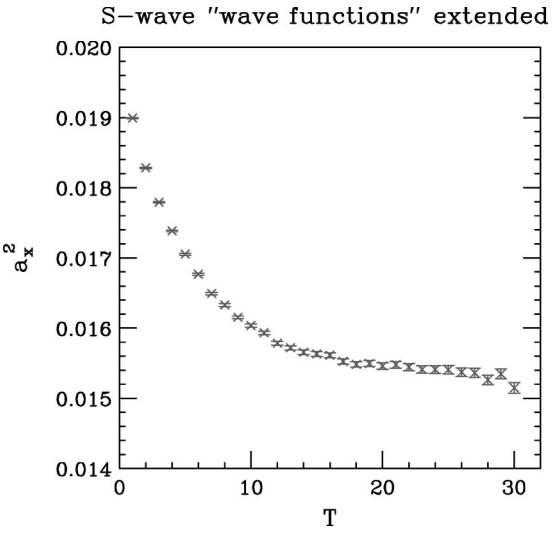


FIG. 2. Effective $a_x^2$ as a function of $T$ for $S$-wave bottomonium.

Our estimates of $\mathcal{F}_1^{\rm VS}/\mathcal{G}_1^{\rm VS}$ from the various discretizations of $\mathbf{D}^2$ are obtained from fits to the propagator ratios of Eq. (12) for the extended source. Our point-source results for

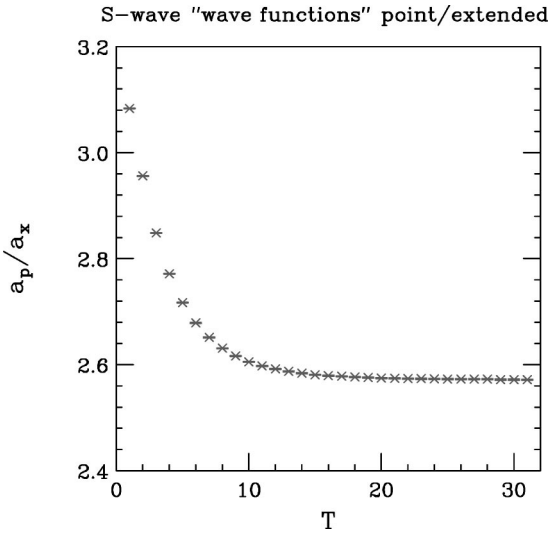


FIG. 3. Ratio of the extended-point propagator to the extended-extended propagator as a function of $T$ for $S$-wave bottomonium.

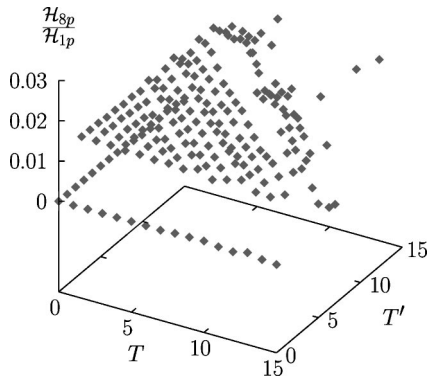


FIG. 4. $\mathcal{H}_{8L}/\mathcal{H}_{1L}$ as a function of $T$ and $T'$ for point sources/sinks. Error bars have been suppressed to make the graph more easily readable. The suffix $p$ indicates that we used a point source and point sink.

these ratios are completely consistent with the extended-source results.

Finally, we extract the ratio $\mathcal{H}_8/\mathcal{H}_1^{\rm VS}$ from the quantity represented in Fig. 1, where the 4-point vertex denotes the octet operator of Eq. (4d). Its value for the case of a point source and sink is plotted in Fig. 4. We consider fits over the ranges $T_1 \leqslant T$, $T' \leqslant T_2$, for all choices of $T_1$ and $T_2$, excluding overlaps. From these we choose a "best" fit, i.e., one with a good confidence level, small error, and a reasonably large range $T_2 - T_1$. The chosen best fit is over the range 2–12 and has a confidence level of 40%. It yields a value $\mathcal{H}_{8L}/\mathcal{H}_{1L} = 0.01565(8)$. In comparison, the fit with the highest confidence level (99.8%) is over the range 6–8 and yields a value $\mathcal{H}_{8L}/\mathcal{H}_{1L} = 0.01540(16)$, which is in agreement the selected fit. The results for the extended source are consistent the results for a point source, but the plateau occurs roughly one unit later in $T, T'$, and the "data" are noisier. We estimate the systematic error in $\mathcal{H}_{8L}/\mathcal{H}_{1L}$ by examining the entire plateau, both for the point-source data and for the extended-source data, and determining the range of fluctuations in the region in which the signal-to-noise ratio is appreciable.

Note that there is clear evidence for a plateau in $\mathcal{H}_{8L}/\mathcal{H}_{1L}$ for $T, T' \gtrsim 1$, and, so, we are justified in assuming that the asymptotic behavior occurs for relatively small $T, T'$, where the signal-to-noise ratio is relatively good. An analysis of the effective wave function for the $P$-wave state shows a plateau that starts at $T \approx 10$. However, we observe in the ratios that we use to calculate $\mathcal{F}_1$, in which we have decent signals out to $T = 31$, that the plateau can start much before effective masses and effective wave functions indicate that one has obtained a pure state. This is also the case for the data that we present later on $G_1/G_1^{\rm VS}$. Presumably, the early onset of a plateau in these ratios indicates that their values are not very different for the $1P$ and $2P$ states (and $1S$ and $2S$ states).

The results for these lattice matrix elements are given in Table I. The first error bar is statistical. The second error bar is a combination of our estimate of the systematic error that arises from our choice of fits and our estimate of the uncertainty that arises from the fact that the propagators have not reached their asymptotic forms in the region of measurement. We note that the dependence on the light-quark mass is weak. For this reason and for the reason that we have fewer configurations at the higher light-quark mass, we have not calculated the $P$-wave matrix elements at $m = 0.025$.

### B. Lattice-to-continuum conversion

First, let us present the one-loop results for the coefficients that relate the lattice matrix elements to their continuum ($\overline{\rm MS}$) counterparts. These coefficients were defined and the method for their calculation was outlined in the Sec. III. The loop integrals were evaluated numerically, using the adaptive Monte Carlo routine VEGAS [11]. The values of the coefficients, in lattice units ($a = 1$), are presented in Table II. These values depend on the value of the bottom-quark mass in lattice units. However, as we have already discussed, we take the bottom-quark mass, in lattice units, to be the same at both the values of the light-quark mass $m$ that we use. Then, with the exception of $\zeta$, the coefficients in Table II depend on the light-quark mass only through the scale of $\alpha_s$, which is proportional to $a$, since $a$ depends (weakly) on $m$. $\zeta$ has additional dependence on $a$ and, hence, on $m$, since it contains a term that is proportional to $\ln(\mu a)$, where $\mu$ is the NRQCD factorization scale. We take $\mu = 4.3$ GeV, which is close to $M_b(\overline{\rm MS})$.

We convert the lattice matrix elements to continuum matrix elements using the formulas of Eqs. (20) and (21). Here, we choose $\alpha_s = \alpha_P(1/a)$, where $\alpha_P$ is defined in Ref. [7]. To convert to physical units, we use $a^{-1} = 2.44$ GeV for $m = 0.01$ and $a^{-1} = 2.28$ GeV for $m = 0.025$, as determined by the NRQCD Collaboration [7] from the $\Upsilon$-$\chi_b$ mass splitting.

TABLE I. Lattice bottomonium decay matrix elements for light quark masses $m = 0.01$ and $m = 0.025$.

| | $m = 0.01$ | $m = 0.025$ |
|---|---|---|
| $\mathcal{G}_{1L}$ | $0.20479 \pm 0.00036 \pm 0.0028$ | $0.21265 \pm 0.00061 \pm 0.0028$ |
| $\mathcal{F}_{1L}({\rm non})/\mathcal{G}_{1L}$ | $1.53074 \pm 0.00049 \pm 0.001$ | $1.54816 \pm 0.00069 \pm 0.0005$ |
| $\mathcal{F}_{1L}({\rm cov})/\mathcal{G}_{1L}$ | $0.99667 \pm 0.00037 \pm 0.0005$ | $1.00740 \pm 0.00049 \pm 0.0005$ |
| $\mathcal{F}_{1L}({\rm non_2})/\mathcal{G}_{1L}$ | $0.86310 \pm 0.00027 \pm 0.0005$ | $0.87226 \pm 0.00037 \pm 0.0003$ |
| $\mathcal{F}_{1L}({\rm cov_2})/\mathcal{G}_{1L}$ | $1.23209 \pm 0.00022 \pm 0.001$ | $1.23961 \pm 0.00029 \pm 0.0005$ |
| $\mathcal{H}_{1L}$ | $0.02016 \pm 0.00078 \pm 0.0014$ | — |
| $\mathcal{H}_{8L}/\mathcal{H}_{1L}$ | $0.01565 \pm 0.00008 \pm 0.001$ | — |

TABLE II. Coefficients relating lattice and continuum matrix elements. The different versions of $\gamma$ and $\phi$ relate to the different discretizations of $\mathbf{D}^2$.

| Coefficient | Value |
|---|---|
| $\epsilon$ | $-0.4387\alpha_s$ |
| $\gamma(\mathrm{non})$ | $-0.9622\alpha_s$ |
| $\gamma(\mathrm{cov})$ | $-2.543\alpha_s$ |
| $\gamma(\mathrm{non}_2)$ | $-0.9489\alpha_s$ |
| $\phi(\mathrm{non})$ | $4.822\alpha_s$ |
| $\phi(\mathrm{cov})$ | $3.729\alpha_s$ |
| $\phi(\mathrm{non}_2)$ | $3.078\alpha_s$ |
| $\iota$ | $-1.232\alpha_s$ |
| $\eta$ | $0.05484\alpha_s$ |
| $\zeta(m=0.01)$ | $-0.01285\alpha_s$ |
| $\zeta(m=0.025)$ | $-0.01680\alpha_s$ |

Then, the required values of $\alpha_s$ are $\alpha_P(2.44\ \mathrm{GeV}) = 0.2941 \pm 0.0070$ and $\alpha_P(2.28\ \mathrm{Gev}) = 0.3056 \pm 0.0076$, respectively. Our continuum matrix elements are given in Table III. The first two error bars arise from the statistical and systematic uncertainties in the lattice calculation. The third error bar is our estimate of the uncertainty from uncalculated two-loop corrections to the coefficients in Table II. This uncertainty is estimated as the greater of $\alpha_s$ times the one-loop contribution and $\alpha_s^2$ times the tree-level coefficient. Clearly this is the dominant uncertainty. In the case of $\mathcal{F}_1$, this uncertainty is magnified because the left side of Eq. (20b) is very close in size to the second term on the right side of Eq. (20b). Consequently, our calculation of $\mathcal{F}_1$ is very imprecise. The lattice operator matrix elements $\mathcal{F}_1(\mathrm{cov})$, $\mathcal{F}_1(\mathrm{non})$, and $\mathcal{F}_1(\mathrm{non}_2)$ all yield values of $\mathcal{F}_1$ that are consistent with zero. Furthermore, the error bars in each case are larger than the differences between the central values. The operator matrix element $\mathcal{F}_1(\mathrm{non}_2)$ yields the smallest uncertainties, and it is the value that derives from this matrix element that we report in Table III.

There are some additional uncertainties that are not included in Table III. One is the uncertainty that arises from the uncertainty in the NRQCD Collaboration's determination of $a$ [7]. We include only the statistical uncertainty in $a^{-1}$ in our calculation. The NRQCD collaboration also reports an order-$a^2$ uncertainty and an order-$v^4$ uncertainty. The former is equivalent, in NRQCD, to the order-$v^2$ uncertainty, which we estimate later. The latter we ignore in comparison with the order-$v^2$ uncertainty in our calculation. The uncertainty in $a$ translates into an uncertainty in $\mathcal{G}_1$ of approximately 8% at $m=0.01$ and 19% at $m=0.025$. In the case of $\mathcal{H}_1$, it leads to an uncertainty of approximately 14% at $m=0.01$. Another uncertainty arises from the neglect of corrections of higher order in $v^2$ in the action. These are nominally of order 10%, but are expected to be much smaller for spin-averaged quantities. (Of course, in order to obtain a spin-averaged value of $\mathcal{G}_1$, one would need to observe the $\eta_b$ and measure its decay width into $\gamma\gamma$.) Finally, there is the effect of order-$a^2$ corrections in the gluon and light-quark sectors, which cause appreciable flavor-symmetry breaking at the values of the lattice spacing that we use. These effects could best be estimated by repeating the calculation at a different value of $\beta$.

### C. Phenomenological value of the matrix element

We obtain a phenomenological estimate for $\mathcal{G}_1$ from the leptonic decay width of $\Upsilon$ [12]

$$\Gamma(\Upsilon \to e^+e^-) \approx \frac{2\pi Q_b^2 \alpha^2}{3M_b^2(\mathrm{pole})}\left(1 - \frac{16\alpha_s}{3\pi}\right)\mathcal{G}_1. \qquad (22)$$

Here, we use $M_b(\mathrm{pole}) = 5.0 \pm 0.2$ GeV [13], $\alpha(M_b) = 1/132$, $\alpha_s(M_b) = 0.212$, and $\Gamma(\Upsilon \to e^+e^-) = 1.32 \pm 0.05$ Gev [14]. The value of $\mathcal{G}_1$ given in Table III includes only the experimental uncertainty.

In extracting the phenomenological value of $\mathcal{G}_1$, we have not included the relative-order-$\alpha_s^2$ correction to $\Gamma(\Upsilon \to e^+e^-)$ [15]. It would be inconsistent to include this correction without also including the order-$\alpha_s^2$ corrections to the short-distance coefficients that relate the lattice operator matrix elements to the continuum ones. The relative-order-$\alpha_s^2$ correction to $\Gamma(\Upsilon \to e^+e^-)$ contains a large dependence on the NRQCD factorization scale $\mu$. If we did include this correction in our extraction, then the phenomenological value of $\mathcal{G}_1$ would range from 3.76 $\mathrm{GeV}^3$ to 8.77 $\mathrm{GeV}^3$ as

TABLE III. Continuum $\overline{\mathrm{MS}}$ bottomonium decay matrix elements from our lattice calculations with two dynamical light quarks ($n_f = 2$) and, for comparison, a phenomenological value of $\mathcal{G}_1$. The error bar on the phenomenological value of $\mathcal{G}_1$ does not include the theoretical uncertainty.

| | Calculation ($n_f=2$) | | |
|---|---|---|---|
| | Lattice units | Physical units | Phenomenology |
| $m=0.01$ | | | |
| $\mathcal{G}_1$ | 0.2351(4)(32)(240) | 3.416(6)(47)(340) $\mathrm{GeV}^3$ | 3.86(14) $\mathrm{GeV}^3$ |
| $\mathcal{F}_1/\mathcal{G}_1$ | $-0.8$–$0.3$ | $-5$–$2$ $\mathrm{GeV}^2$ | — |
| $\mathcal{H}_1$ | 0.032(1)(2)(5) | 2.7(1)(2)(5) $\mathrm{GeV}^5$ | — |
| $\mathcal{H}_8/\mathcal{H}_1$ | 0.01354(5)(63)(390) | 0.002275(9)(105)(660) $\mathrm{GeV}^{-2}$ | — |
| $m=0.025$ | | | |
| $\mathcal{G}_1$ | 0.2456(7)(32)(270) | 2.911(8)(38)(320) $\mathrm{GeV}^3$ | 3.86(14) $\mathrm{GeV}^3$ |
| $\mathcal{F}_1/\mathcal{G}_1$ | $-0.9$–$0.3$ | $-4.7$–$1.5$ $\mathrm{GeV}^2$ | — |

the $\mu$ ranges from 1 GeV to $M_b$. This large $\mu$ dependence and the large size of the correction at $\mu = M_b$ would seem to indicate that the uncertainty in the phenomenological value may be close to 100%. However, experience with one-loop corrections to quarkonium decay processes suggests that such large corrections may be canceled by the order-$\alpha_s^2$ corrections to the short-distance coefficients that relate the lattice operator matrix elements to the continuum ones. Certainly, the large $\mu$ dependence in the relative-order-$\alpha_s^2$ correction to $\Gamma(\Upsilon \to e^+e^-)$ would be compensated exactly by a large $\mu$ dependence in the order-$\alpha_s^2$ corrections to the short-distance coefficients.

The uncertainty in the phenomenological value of $\mathcal{G}_1$ that arises from the uncertainty in the value of $M_b$ is about 8%. This is negligible in comparison with the uncertainty associated with the perturbation expansion. Given present theoretical uncertainties, it is not yet possible to extract $\mathcal{F}_1$ from experiment.

$\mathcal{H}_1$ and $\mathcal{H}_8$ are related to the $\chi_b$ decay widths, which have not yet been determined in experiments. Large corrections to the perturbation series [16] are likely to be important sources of uncertainty in the determination of these quantities, once experimental data become available.

### D. Extrapolation to physical light-quark values

We use linear extrapolation methods to estimate the calculated matrix elements at the physical values of the light-quark masses and at the physical number of light-quark flavors. Extrapolating to $m=0$, we find that $\mathcal{G}_1 = 3.75(1)(8)(38)$ GeV$^3$. To extrapolate to the physical values of the light-quark masses, we use the HEMCGC light-hadron spectroscopy measurements on the gauge configurations that we employ [10] to estimate that one-third the mass of the strange quark is approximately 0.0071, in lattice units. Then, we extrapolate $\mathcal{G}_1$ to this value of $m$. Note that, since we are using linear extrapolations in both $m$ and the number of flavors, this procedure yields the same result as would setting $m_s = 0.02$ and $m_u = m_d = 0$. Finally, we use our results for quenched QCD at $\beta = 6.0$ [3] to extrapolate to three light-quark flavors, obtaining $\mathcal{G}_1 = 4.10(1)(9)(41)$ GeV$^3$. This result is approximately 6% higher than the phenomenological value. Similarly, extrapolations to three light-quark flavors (with no extrapolation in $m$) yield $\mathcal{H}_1 \approx 3.3$ GeV$^5$ and $\mathcal{H}_8/\mathcal{H}_1 \approx 0.0018$ GeV$^{-2}$.

### E. Tests of the vacuum-saturation approximation

Our lattice calculations permit us to test the validity of the vacuum-saturation approximation for $\mathcal{G}_1$ and $\mathcal{H}_1$. NRQCD predicts that

$$\mathcal{G}_1/\mathcal{G}_1^{\rm VS} = 1 + \mathcal{O}(v^4) \tag{23}$$

$$\mathcal{H}_1/\mathcal{H}_1^{\rm VS} = 1 + \mathcal{O}(v^4). \tag{24}$$

Note that, although our lattice action is accurate only to leading order in $v$, it *does* contain interactions of relative order $v^2$, which arise through the terms proportional to the gauge field in the covariant derivatives. These interactions allow for the spin-independent emission of transverse gluons, which produces the leading correction to the vacuum-saturation approximation.[3]

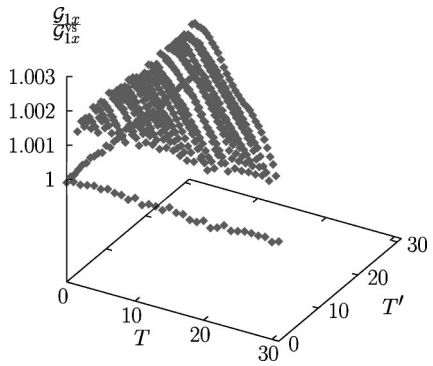


FIG. 5. The ratio $\mathcal{G}_{1L}/\mathcal{G}_{1L}^{\rm VS}$ as a function of $T$ and $T'$, where the subscript $x$ indicates the use of an extended source. The error bars have been suppressed for clarity of presentation.

In order to test the relations (23) and (24), we need to observe a plateau in ratios of the form of Fig. 1. We have measured these ratios with both point and extended sources. The detailed method of analysis is similar to that for the ratio $\mathcal{H}_{8L}/\mathcal{H}_{1L}$ described above. Because $\mathcal{G}_1 \propto \mathcal{G}_{1L}$ and $\mathcal{H}_1 \propto \mathcal{H}_{1L}$, up to corrections of relative order $\alpha_s$, we use the lattice quantities to evaluate the ratios in Eqs. (23) and (24). We find that

$$\mathcal{G}_1/\mathcal{G}_1^{\rm VS} = 1.0017(1) \tag{25}$$

$$\mathcal{H}_1/\mathcal{H}_1^{\rm VS} = 1.0049(2). \tag{26}$$

These results are consistent with $v^2$ being of order 0.1 and justify our use of the vacuum-saturation approximation in computing matrix elements. Figure 5 shows the plateau in the ratio of lattice matrix elements $\mathcal{G}_{1L}/\mathcal{G}_{1L}^{\rm VS}$. We note that the plateau is reached for $T, T' \gtrsim 1$.

### F. The nonrelativistic energy

For comparison with the work of the NRQCD Collaboration, we give our estimate for their "energy" $E_{NR}$ [4], which is related to the $E_S$ of Eq. (9) by

$$E_{NR} = E_S + 2 \ln u_0. \tag{27}$$

For $m = 0.01$ we obtain $E_{NR} = 0.4841(2)$, and for $m = 0.025$ we obtain $E_{NR} = 0.4901(3)$ (statistical errors only). This is to be compared with the value $E_{NR} = 0.493(1)$ ($m$ unspecified)

[3]The inclusion of covariant derivatives does not, of course, generate all of the relative-order-$v^2$ contributions to the matrix elements we consider. In particular, the action that we use contains none of the spin-dependent terms that distinguish states with the same orbital angular momentum but with different total angular momentum (such as the $\Upsilon$ and the $\eta_b$).

that was obtained by the NRQCD Collaboration [13] using an action that is accurate through next-to-leading order in $v^2$.

## V. DISCUSSION AND CONCLUSIONS

We have measured, in lattice simulations with two light-quark flavors, the matrix elements of leading order and next-to-leading order in $v^2$ that mediate the decays of the $\Upsilon$ and the color-singlet and color-octet matrix elements of leading order in $v^2$ that mediate the decays of the $\chi_b$ states. We have also computed the relations between the lattice matrix elements and continuum ($\overline{\rm MS}$) matrix elements to one-loop accuracy and have converted our lattice results to continuum results. We have extrapolated these results to the case of three light-quark flavors.

Our measured value of the lowest-order $\Upsilon$-decay matrix element, extrapolated to three flavors, is $\mathcal{G}_1 = 4.10(1)(9)(41)$ GeV$^3$. This is in good agreement with the phenomenological value $\mathcal{G}_1 = 3.86(14)$, which we extracted from the experimental value for the leptonic decay width by using the perturbative-QCD expression for the leptonic decay width, accurate through relative order $\alpha_s$. This contrasts with the value for $\mathcal{G}$ that we obtained in the quenched approximation [3], which is 40–45 % lower than the phenomenological value. The large size and large scale dependence of the order-$\alpha_s^2$ correction to the leptonic width [15] suggest that the theoretical uncertainty in the phenomenological value of the matrix element may be quite large. However, one can utilize the order-$\alpha_s^2$ correction consistently only when one has incorporated two-loop corrections into the coefficients for the lattice-to-continuum conversion. Then the scale dependence would be compensated exactly, and some of the large correction would likely be canceled.

At present, the most that we can say about the next-to-leading-order $\Upsilon$-decay matrix element $\mathcal{F}_1$ is that the continuum ($\overline{\rm MS}$) matrix element is probably negative. Notice that, although the lattice matrix element is strictly positive, the subtractions involved in converting it to a continuum matrix element can, and apparently do, change its sign. If this result is maintained at higher orders in perturbation theory, then it is clear that any simple potential model, which must, of necessity, give a positive result, cannot yield the correct values for such higher-order matrix elements.

We find that the value of the color-singlet $P$-wave matrix element $\mathcal{H}_1$ for three light-quark flavors is roughly 70% higher than the quenched value. The color-octet contribution to the $P$-wave decays, which is mediated by $\mathcal{H}_8$, arises from a distinctive QCD effect: the process in which the $b\overline{b}$ color-singlet $P$-wave state fluctuates into a $b\overline{b}$ color-octet $S$-wave state plus a soft gluon. Such a contribution is absent in simple potential models. We find that the value of $\mathcal{H}_8$ for three light-quark flavors is about 40% larger than the quenched value, but that the value of the ratio $\mathcal{H}_8/\mathcal{H}_1$ for three light-quark flavors is approximately 14% lower than the quenched value. According to the velocity-scaling rules, both $\mathcal{H}_1$ and $\mathcal{H}_8$ are of order $v^4$ (Ref. [1]). Therefore, we expect $M_b^2\mathcal{H}_8/\mathcal{H}_1$ to be of order unity times a factor $1/(2N_c)$, where $N_c=3$ is the number of QCD colors, to account for the spin and color traces in the definition of $\mathcal{H}_1$ (Ref. [17]). Our result for $M_b^2\mathcal{H}_8/\mathcal{H}_1$ is smaller than this estimate by about a factor of three. Our values for $\mathcal{H}_1$ and $\mathcal{H}_8$ could be used to make predictions for the, as yet, unmeasured $\chi_b$ decay rates. However, as we have mentioned, large next-to-leading-order corrections in the perturbation series for those decay rates [16] suggest that further theoretical progress may be necessary in order to achieve a precise comparison with experiment.

Our results indicate that the quenched approximation yields a poor estimate of the NRQCD matrix elements. As we have mentioned, the trends in going from the quenched approximation to the physical number of light-quark flavors can be understood in terms of a simple picture. The lattice spacing and heavy-quark mass are determined by fitting to bottomonium spectroscopy, which probes the wave functions at distances of order $1/(M_b v)$. On the other hand, the decay matrix elements sample the wave function and its derivatives at much shorter distances, of order $a$. In the absence of the sea of light quark-antiquark pairs, the strong coupling constant runs too fast, becoming too small at the shorter distance. This leads to an underestimate of the decay matrix elements, since the values of the wave function and its derivatives depend on the strength of the potential at short distances. We note that the $S$-wave matrix elements $G_1$ and $H_8$ both increase by about the same fraction in going from the quenched approximation to three light-quark flavors, while the $P$-wave matrix element $H_1$ increases by a larger fraction. This may be because $P$-wave matrix elements depend on the derivative of the wave function at the origin, as opposed to the wave function at the origin, and, so, are more sensitive to changes in the strength of the potential at short distances.

In order to improve the lattice estimates of the matrix elements for $S$- and $P$-wave bottomonium decay, one would first need more precise measurements of the lattice spacing $a$. A more stringent comparison with experiment would also require a more precise determination of the bottom-quark mass $M_b$, as well as a calculation to two-loop accuracy of the perturbative coefficients that relate the lattice matrix elements to the continuum matrix elements.[4] In the case of $\mathcal{F}_1$ this last improvement is essential to obtain a useful prediction of the continuum matrix element. Beyond this it would be valuable to use gauge-field configurations that have been generated with improved actions. Only when this has been done could one justify using NRQCD actions that have been improved to higher orders in $v$ and $a$ for the extraction of bottomonium decay matrix elements.

## ACKNOWLEDGMENTS

We wish to thank the NRQCD Collaboration, and especially G. P. Lepage, for discussions of their published and

[4] Alternatively, one could carry out a non-perturbative (lattice) calculation of these coefficients or compute the short-distance decay coefficients in lattice perturbation theory, rather than in continuum perturbation theory.

unpublished results. We thank K. Hornbostel for the use of his 3-loop program for evolving $\alpha_s$. We also thank the HEMCGC Collaboration and, in particular, U. M. Heller for giving us access to their gauge-field configurations. The lattice calculations were performed on the Cray J90's at NERSC. Work in the High Energy Physics Division at Argonne National Laboratory is supported by the U.S. Department of Energy, Division of High Energy Physics, under Contract No. W-31-109-ENG-38. S.K. is supported by Korea Research Foundation Grant KRF-2001-015-DP0088.

[1] G. T. Bodwin, E. Braaten, and G. P. Lepage, Phys. Rev. D **51**, 1125 (1995); **55**, 5853(E) (1997).
[2] G. T. Bodwin, E. Braaten, and G. P. Lepage, Phys. Rev. D **46**, 1914 (1992).
[3] G. T. Bodwin, S. Kim, and D. K. Sinclair, Nucl. Phys. B (Proc. Suppl.) **34**, 434 (1994); **42**, 306 (1995); G. T. Bodwin, D. K. Sinclair, and S. Kim, Phys. Rev. Lett. **77**, 2376 (1996); Int. J. Mod. Phys. A **12**, 4019 (1997).
[4] C. T. Davies, K. Hornbostel, A. Langnau, G. P. Lepage, A. Lidsey, J. Shigemitsu, and J. H. Sloan, Phys. Rev. D **50**, 6963 (1994).
[5] G. P. Lepage (private communication).
[6] G. P. Lepage, L. Magnea, C. Nakhleh, U. Magnea, and K. Hornbostel, Phys. Rev. D **46**, 4052 (1992).
[7] C. T. Davies, K. Hornbostel, G. P. Lepage, P. McCallum, J. Shigemitsu, and J. H. Sloan, Phys. Rev. D **56**, 2755 (1997).
[8] G. T. Bodwin, S. Kim, and D. K. Sinclair (in preparation).
[9] G. T. Bodwin and Y. Chen, Phys. Rev. D **60**, 054008 (1999).
[10] K. M. Bitar *et al.*, Phys. Rev. D **49**, 6026 (1994).
[11] G. P. Lepage, J. Comput. Phys. **27**, 192 (1978).
[12] R. Barbieri, R. Gatto, R. Kogerler, and Z. Kunszt, Phys. Lett. **57B**, 455 (1975); W. Celmaster, Phys. Rev. D **19**, 1517 (1979).
[13] C. T. Davies *et al.*, Phys. Rev. Lett. **73**, 2654 (1994).
[14] Particle Data Group, D. E. Groom *et al.*, Eur. Phys. J. C **15**, 1 (2000).
[15] M. Beneke, A. Signer, and V. A. Smirnov, Phys. Rev. Lett. **80**, 2535 (1998).
[16] R. Barbieri, M. Caffo, and E. Remiddi, Nucl. Phys. **B162**, 220 (1980); R. Barbieri, M. Caffo, R. Gatto, and E. Remiddi, *ibid.* **B192**, 61 (1981); A. Petrelli, Phys. Lett. B **380**, 159 (1996); H. Huang and K. Chao, Phys. Rev. D **54**, 6850 (1996); **56**, 1821(E) (1997); E. Braaten and Y. Chen, *ibid.* **55**, 7152 (1997).
[17] A. Petrelli, M. Cacciari, M. Greco, F. Maltoni, and M. L. Mangano, Nucl. Phys. **B514**, 245 (1998).